Supplementary Material

Further details of the methodologies used in this study is presented herein. This document covers the following: FeMRA imaging details; calculation of the initial prism layer height; grid convergence calculation equations; mesh base size validation for LES; calculated physiological flow-splits using the 'splitting method'; calculated Windkessel values in proximal-to-fistula study; non-Newtonian blood flow model; and the Q-Criterion.

FeMRA imaging details

The information of the FeMRA imaging protocol used for ascertaining the datasets of this investigation were as per Table 1.

Table 1: FeMRA imaging details

Scan	VENC (cm/s)	TE (ms)	TR (ms)	Slice thickness (mm)	FOV (mm)	Resolution (pixels per mm)	WL	WW
Chest	-	1.03	2.86	3	325x400	0.96	138	348
Upper Arm	-	1.53	4.5	3	300x480	1.40	139	379
Lower Arm	-	1.64	4.7	3	175x400	1.68	112	319
PC Proximal*	150	2.47	A5 5∼s	3	340x234	0.565	157	394
PC Distal*	150	2.47	A5 5∼s	3	340x234	0.565	158	391

*where PC represents Phase-Contrast

Calculation of initial prism layer height

Based on the desired y+ and the fluid properties, the frictional velocity (u_T), WSS (τ_w), and the skin friction coefficient (C_f) can be calculated as per Equations 1-4 for estimating the first prism cell height of the mesh, similarly to Johnston et al.[4] The values computed through the use of Equations 1-4 are given in Table 2.

$$y+ = \frac{\rho.u_T.y}{\mu} \tag{1}$$

$$u_T = \sqrt{\frac{\tau_w}{\rho}} \tag{2}$$

$$\tau_w = \frac{1}{2}.C_f.\rho.U^2 \tag{3}$$

$$C_f = [2log_{10}(Re_x) - 0.65]^{-2.3} \tag{4}$$

Table 2: Values used for the initial hybrid mesh generation

Aortic D (m)	Re (No units)	C_f (No units)	τ_w (Pa)	u_T (m/s)	Δy_1 (m)
0.0253	4291	0.0130	2.15	0.0451	7.323E-05

Grid convergence calculation equations

The calculation of the grid convergence index (GCI) between three mesh densities, further elaborated on in Steffen et al.[5], was calculated in this study using Equations 5-8.

The order of convergence, P, was calculated as per:

$$P = ln\frac{f_3 - f_2}{f_2 - f_1}/ln(r) \tag{5}$$

where r is the refinement ratio, and f1-f3 are the results ascertained using the varying mesh resolutions.

The Richardson extrapolation is used to predict value at h=0, as per:

$$f_{h=0} = f_{fine} + \frac{f_1 - f_2}{r^P - 1} \tag{6}$$

The calculation of grid convergence index (GCI) for the medium and fine mesh densities is as follows:

$$GCI = \frac{F_s|e|}{r^P - 1} \tag{7}$$

where e is the error between the two mesh, and F_s is an option safety factor.

The asymptotic range of convergence (which should be approximately equal to 1), is calculated as per:

$$\frac{GCI_{2,3}}{r^P \times GCI_{1,2}} \approx 1 \tag{8}$$

Mesh base size validation for LES

The Kolmogorov and Taylor Micro scales were used for ascertaining a reference for the necessary mesh resolution for this study. The calculation of the base size adhered to the necessary specification determined by the calculation of the Kolmogorov and Taylor mirco scales (Fig. 1, Table 3).

Table 3: Maximum length scale values ascertained from a steady-state RANS simulation using the mesh calculated from performing GCI calculations.

Wall Y+	Kolmogorov length scale (m)	Taylor Mirco Scale (m)
0.36	0.00058	0.0031

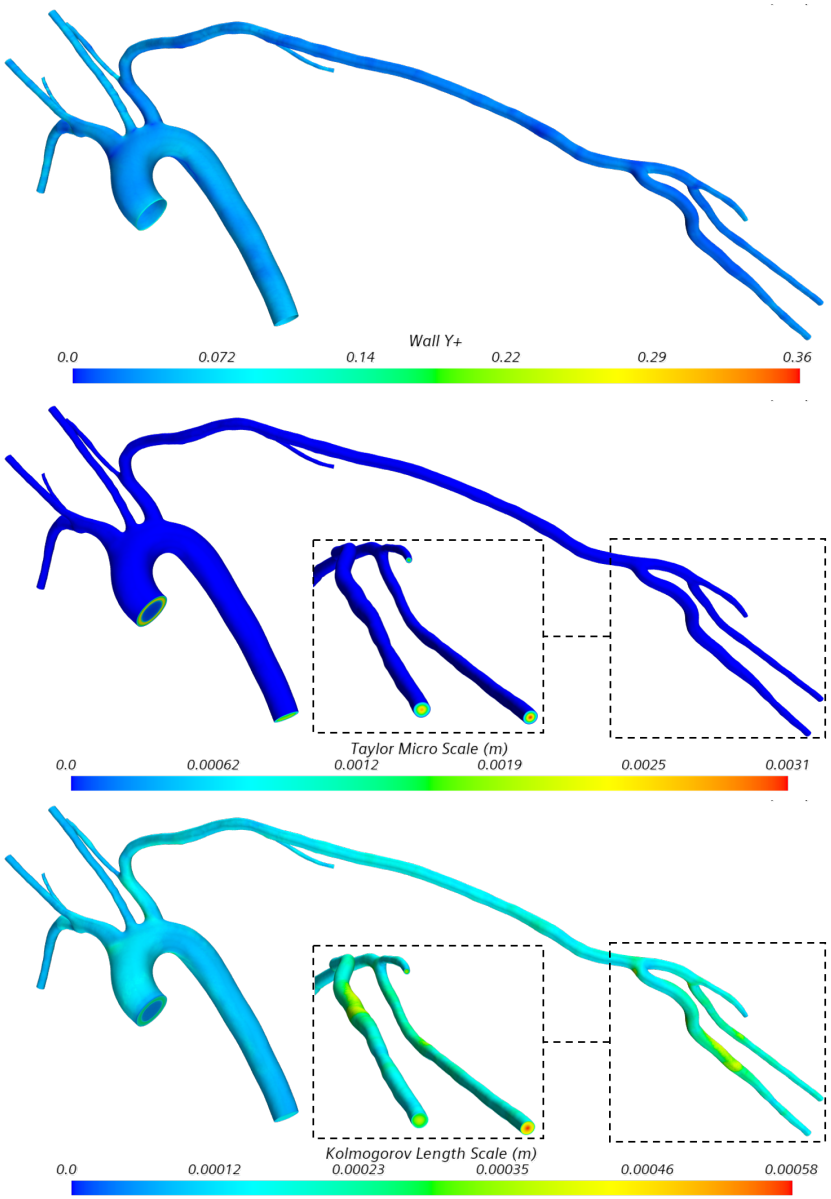

Figure 1: Wall Y+, Taylor Mirco scale, and Kolmogorov length scale of the post-AVF geometry.

The calculated and implemented base size of the mesh (3.8E-4m) was considered appropriate, due to the value being less than the maximum Kolmogorov and Taylor mirco scale values (Fig. 1). Typically, the Kolmogorov scale gives a mesh refinement appropriate for direct numerical simulation (DNS). The Taylor micro scale gives an upper limit for cell size, where the cell size is inappropriate for the SGS model.

Calculated physiological flow-splits using the 'splitting method'

The 'splitting method' described in Chnafa et al.[3] was used in the study as a comparison for the three-element Windkessel models, which were used for assigning pressure outlet boundary conditions. The method works by comparing the diameters of daughter vessel branches immediately following a bifurcation. The percentage flow splits of each bifurcation are subsequently summed along each centreline leading to an outlet. Fig. 2 demonstrates an example of the cross-sectional areas used for calculating the averaged diameters of each branch, which were then used for generating the 'flow split' percentages given in Table 4.

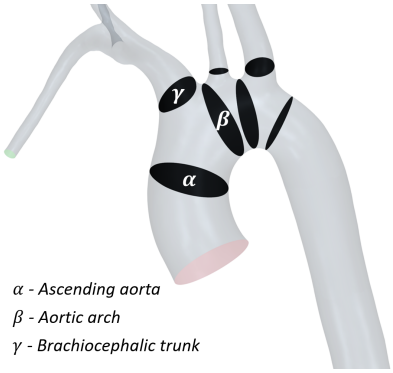

Figure 2: Wall Y+, Taylor Mirco scale, and Kolmogorov length scale of the post-AVF geometry.

Table 4: Calculated physiological flow-splits

Outlet	Flow split (% of cardiac input)
Descending aorta (DA)	71.9
Right subclavian (RSA)	6.4
Right vertebral (RVA)	1.8
Right common carotid (RCC)	5.7
Left common carotid (LCC)	5.9
Left vertebral (LVA)	1.8
Left deep brachial (DBA)	0.4
Left radial (LRA)	3.2
Left interosseous (LIA)	1.1
Left ulnar (LUA)	1.8

Calculated windkessel values in proximal-to-fistula study

The values calculated for the Windkessel models in the proximal-to-fistula haemodynamic study (Table 5) were calculated using the methodology proposed in Alastruey et al.[1]. These values are the same for pre- and post-AVF, with the exception of the boundary condition at the radial artery post-surgically.

Table 5: Calculated Windkessel values for proximal-to-fistula case

Outlet	R $*10^{10}$ $(Pa.s.m^-3)$	C $*10^{-10}$ $(m^3.Pa^-1)$	Z $*10^9$ $(Pa.s.m^-3)$
Descending aorta (DA)	0.02	5.040	0.03
Right subclavian (RSA)	0.24	0.256	0.41
Right vertebral (RVA)	0.85	0.205	1.45
Right common carotid (RCC)	0.30	0.523	5.13
Left common carotid (LCC)	0.23	0.978	4.01
Left vertebral (LVA)	0.85	0.204	1.45
Left deep brachial (DBA)	2.22	0.044	3.81
Left radial (LRA)*	0.45	0.602	0.77
Left interosseous (LIA)	1.73	0.057	2.97
Left ulnar (LUA)	1.00	0.215	1.71

* modified in the post-AVF proximal-to-fistula simulation as described in the paper.

Non-Newtonian Blood model

A non-Newtonian generalised Carreau-Yasuda model[2,6] was used for approximating the properties of blood in the 'Haemodynamics at the AVF anastomosis' simulation; as per:

$$\mu(\dot{\gamma}) = \mu_\infty + (\mu_0 - \mu_\infty)(1 + (\lambda\dot{\gamma})^a)^{(n-1)/a} \tag{9}$$

where a is the shear-thinning control parameter, λ is the relaxation time, μ_0 is the zero shear viscosity, μ_∞ is the infinite shear viscosity, n is the power constant, and $\dot{\gamma}$ is the shear rate. The parameters used in the simulations were as follows: $a = 0.5$, $\lambda = 46.5$/s, $\mu_0 = 150$mPas, $\mu_\infty = 3.5$mPas, $n = 0.342$.

Q-Criterion

The Q-Criterion, a scalar used in the visualisation of vortical flow structures in turbulent fields, is defined by Equation 10. A positive value implies that the flow is vorticity-dominated.

$$Q = \frac{1}{2}(||\Omega||^2 - ||S||^2) \tag{10}$$

where Ω is the spin tensor, and S is the strain-rate tensor.

References

[1] Alastruey Arimon, J. Numerical modelling of pulse wave propagation in the cardiovascular system: development, validation and clinical applications. PhD thesis, Imperial College London, UK, 2006

[2] Carreau, P.J. "Rheological equations from molecular network theories", J. Rheol., 16(1), pp. 99-127. 1972.

[3] Chnafa, C., et al. Better than nothing: A rational approach for minimizing the impact of outflow strategy on cerebrovascular simulations. Am J Neuroradiol. 39(2):337-343, 2018.

[4] Johnston, L., et al. Hemodynamic abnormalities in the aorta of turner syndrome girls. Front. Cardiovasc. Med. 8:670841, 2021.

[5] Steffen, C.J. Jr., et al. "Analysis of Flowfield from a Rectangular Nozzle with Delta Tabs", AIAA 95-2146, 1995.

[6] Yasuda, K. Investigation of the analogies between viscometric and linear viscoelastic properties of polystyrene fluids. PhD Thesis, Dept. of Chemical Engineering, Massachusetts Institute of Technology. 1979.